Supporting Information

High Anodic Performance of Co 1,3,5-Benzenetricarboxylate Coordination Polymers for Li-Ion Battery

Chao Li,[†] Xiaobing Lou,[†] Ming Shen,[†] Xiaoshi Hu,[†] Zhi Guo,[‡] Yong Wang,[‡,*] Bingwen Hu,[†,*] and Qun Chen[†]

[†]*School of Physics and Materials Science, Shanghai Key Laboratory of Magnetic Resonance, Engineering Research Center for Nanophotonics & Advanced Instrument (Ministry of Education), Institute of functional materials, East China Normal University, Shanghai 200062, PR China.*
[‡]*Shanghai Synchrotron Radiation Facility (SSRF), Shanghai 201204, PR China.*

Corresponding Author

*(B.H.) E-mail: bwhu@phy.ecnu.edu.cn.

*(Y.W.) E-mail: wangyong@sinap.ac.cn.

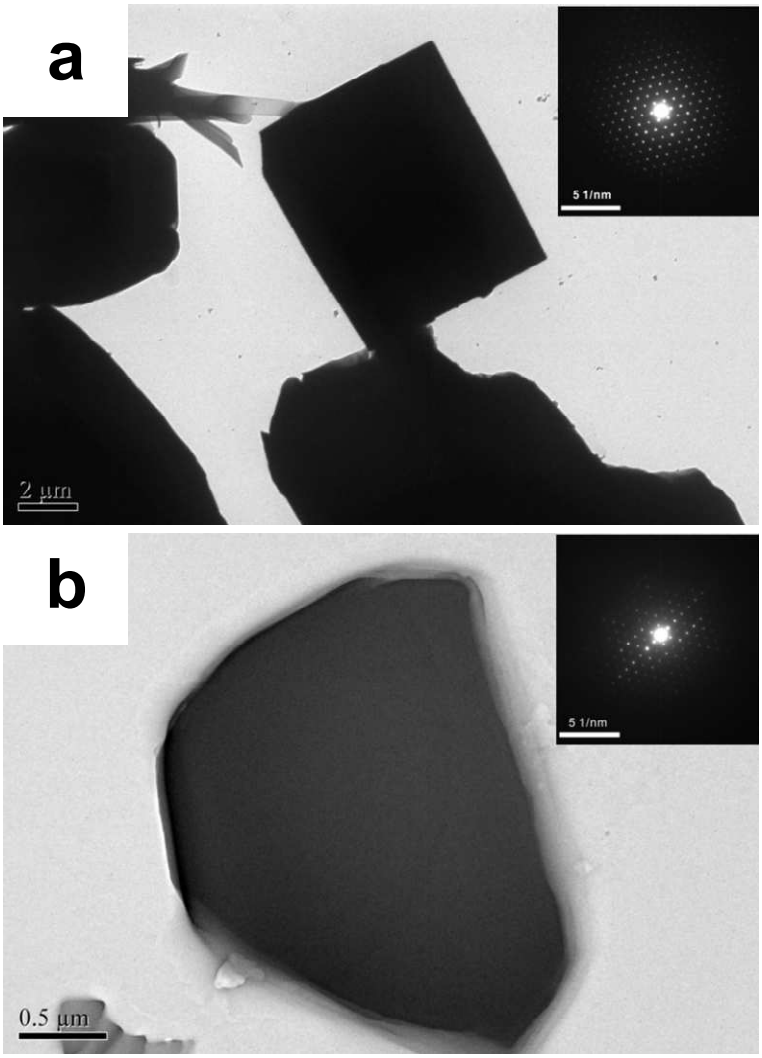

Figure S1. TEM micrographs and the corresponding SAED patterns of CoBTC-DMF (a) and CoBTC-DMF/EtOH (b). The uniform-contrast TEM images of CoBTC-DMF and CoBTC-DMF/EtOH clearly demonstrate their solid and dense nature without discernible porosities.

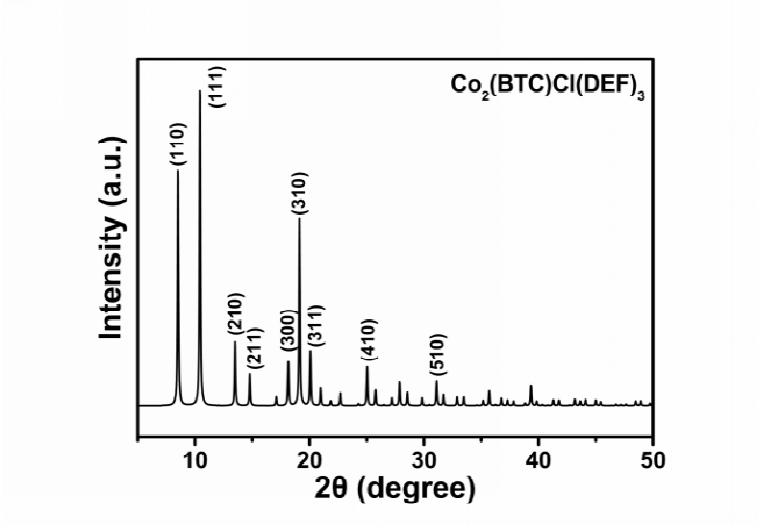

Figure S2. XPRD patterns of $Co_2(BTC)Cl(DEF)_3$.

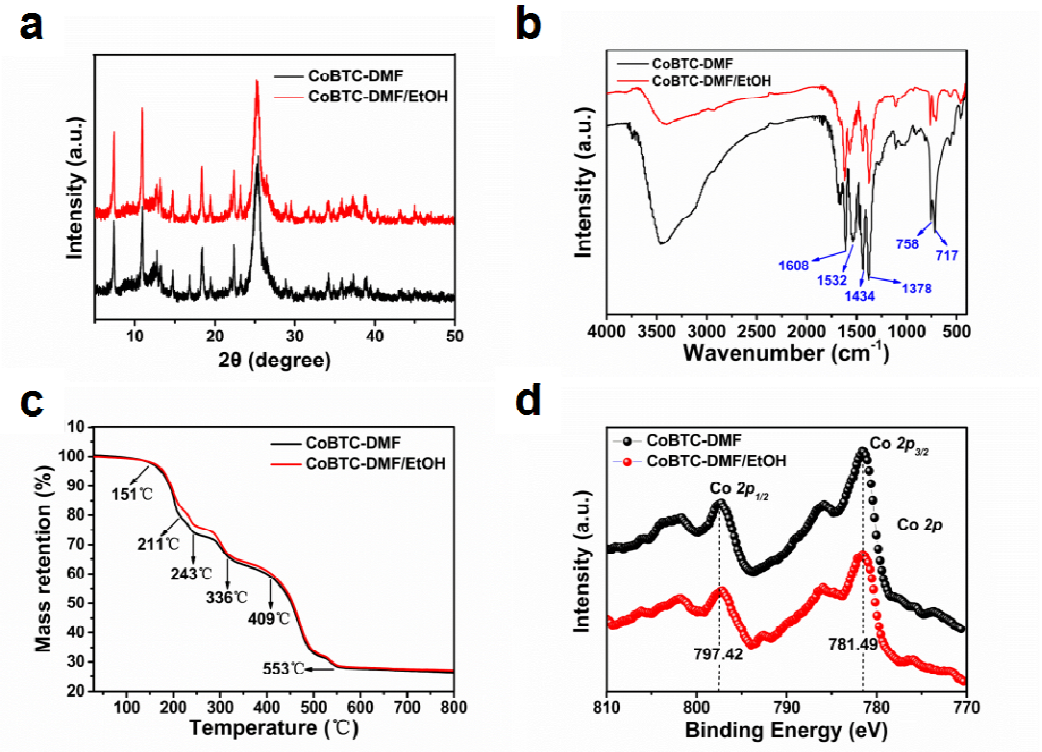

Figure S3. (a) XPRD patterns of CoBTC-DMF and CoBTC-DMF/EtOH. The two samples show peaks located at nearly the same angles, and the peaks are sharp and strong, suggesting a relatively high crystallinity. (b) FT-IR spectra of CoBTC-DMF

and CoBTC-DMF/EtOH. The peaks in the regions of 1608-1532 cm^{-1} can be assigned to the asymmetric stretching vibrations of the carboxylate groups, while the peaks in the regions of 1434-1378 cm^{-1} can be assigned to the symmetric stretching vibrations of the carboxylate groups. The absence of the sharp absorption band from the vibrations of hydroxide (~3600 cm^{-1}) indicate that EtOH molecules are not incorporated in CoBTC-DMF/EtOH. (c) TGA curves of CoBTC-DMF and CoBTC-DMF/EtOH under nitrogen atmosphere. It can be observed that the thermal behaviors of CoBTC-DMF and CoBTC-DMF/EtOH are much different from CoBTC-EtOH. Specifically, the weight loss between 151 and 211 °C can be assigned to the removal of H_2O and DMF molecules adsorbed to the surface and those occluded inside the pores, while the weight loss between 243 and 336 °C can be assigned to the removal of coordinated DMF molecules. The gasification of the BTC ligands begins at 409 °C and after the complete break-down of BTC ligands at ca. 553 °C, the remanent materials are then converted to Co_3O_4. (d) High-resolution Co 2p XPS spectra of CoBTC-DMF and CoBTC-DMF/EtOH, from which the existence of Co^{2+} are also demenstrated.

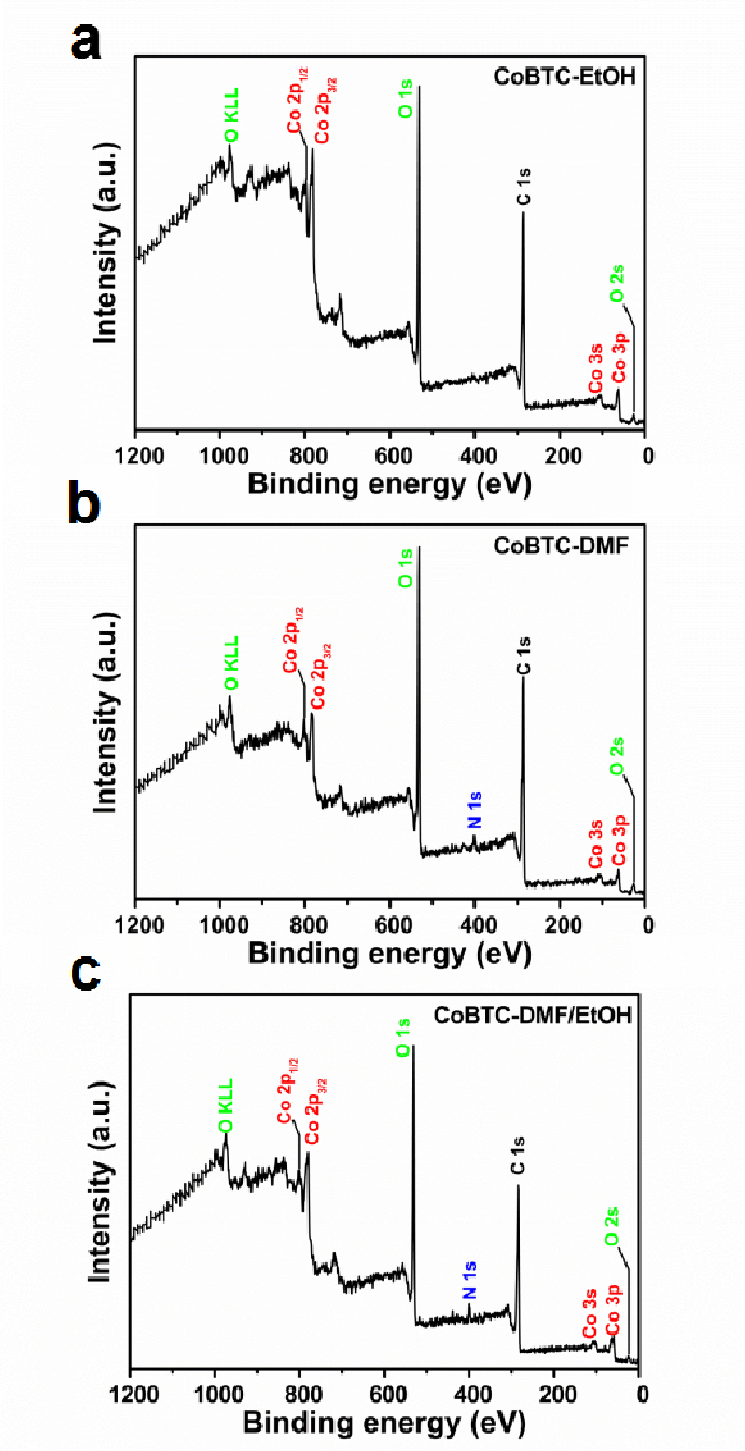

Figure S4. XPS surveys of CoBTC-EtOH (a), CoBTC-DMF (b), and CoBTC-DMF/EtOH (c). The expected N element is detected in CoBTC-DMF and CoBTC-DMF/EtOH, suggesing the exsistence of coordinated DMF in them.

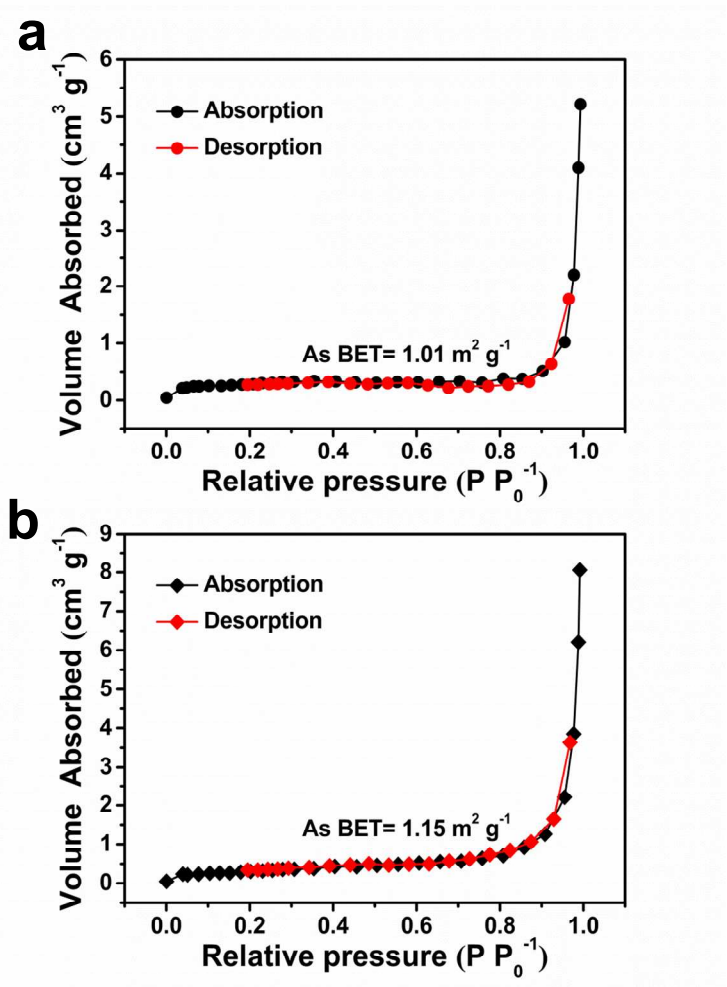

Figure S5. Nitrogen adsorption-desorption isotherms of CoBTC-DMF (a) and CoBTC-DMF/EtOH (b). The BET areas of CoBTC-DMF and CoBTC-DMF/EtOH are 1.01 and 1.15 m^2/g, respectively, which indicate that the two samples have a negligible porosity.

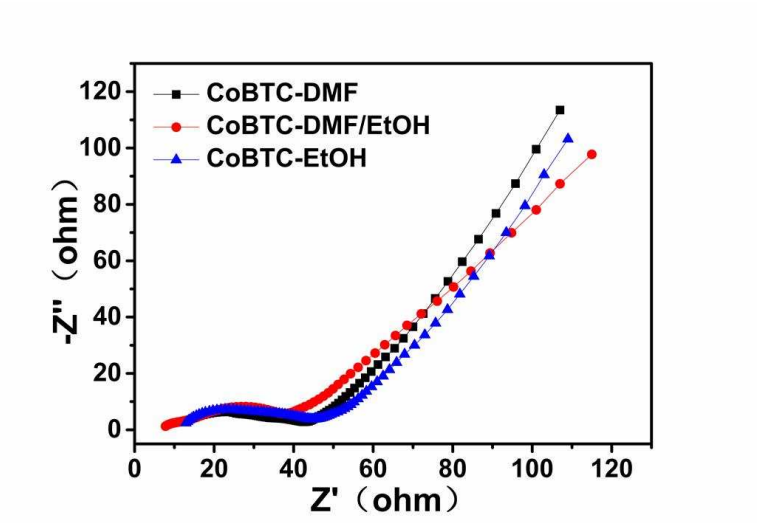

Figure S6. EIS spectra of the CoBTC-EtOH, CoBTC-DMF, and CoBTC-DMF/EtOH electrodes at the 100th cycle. It is clearly observed that the R_{ct} for the CoBTC-EtOH, CoBTC-DMF, and CoBTC-DMF/EtOH electrodes at the 100th cycle are significantly small (<40 Ω), which illustrate the superior cycling performances of the three anodes as well as imply a limited growth of SEI layer and fast solid-state Li^+ diffusion rate in these electrodes during cycling processes.

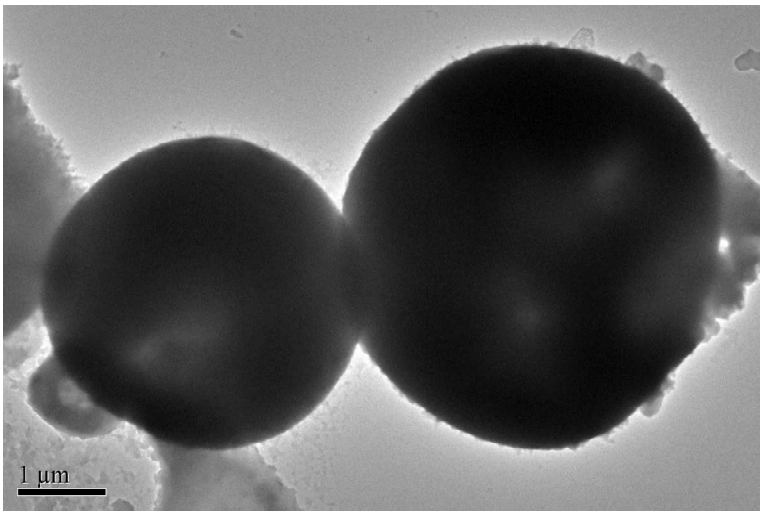

Figure S7. Ex-situ TEM image of the CoBTC-EtOH electrode at the fully lithiated state after rate test. The microsphere morphology of CoBTC-EtOH is largely retained after repetitive cycling.

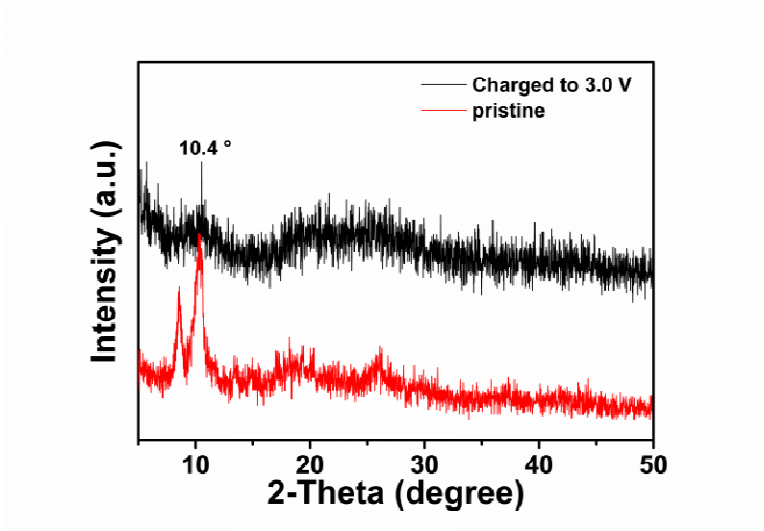

Figure S8. XPRD patterns of the charged CoBTC-EtOH, the patterns of the pristine CoBTC-EtOH were also presented. The diffraction peak at 2θ= 10.4° is detected for the charged sample, suggesting a similar crystal structure after one galvanostatic charge/discharge cycling.

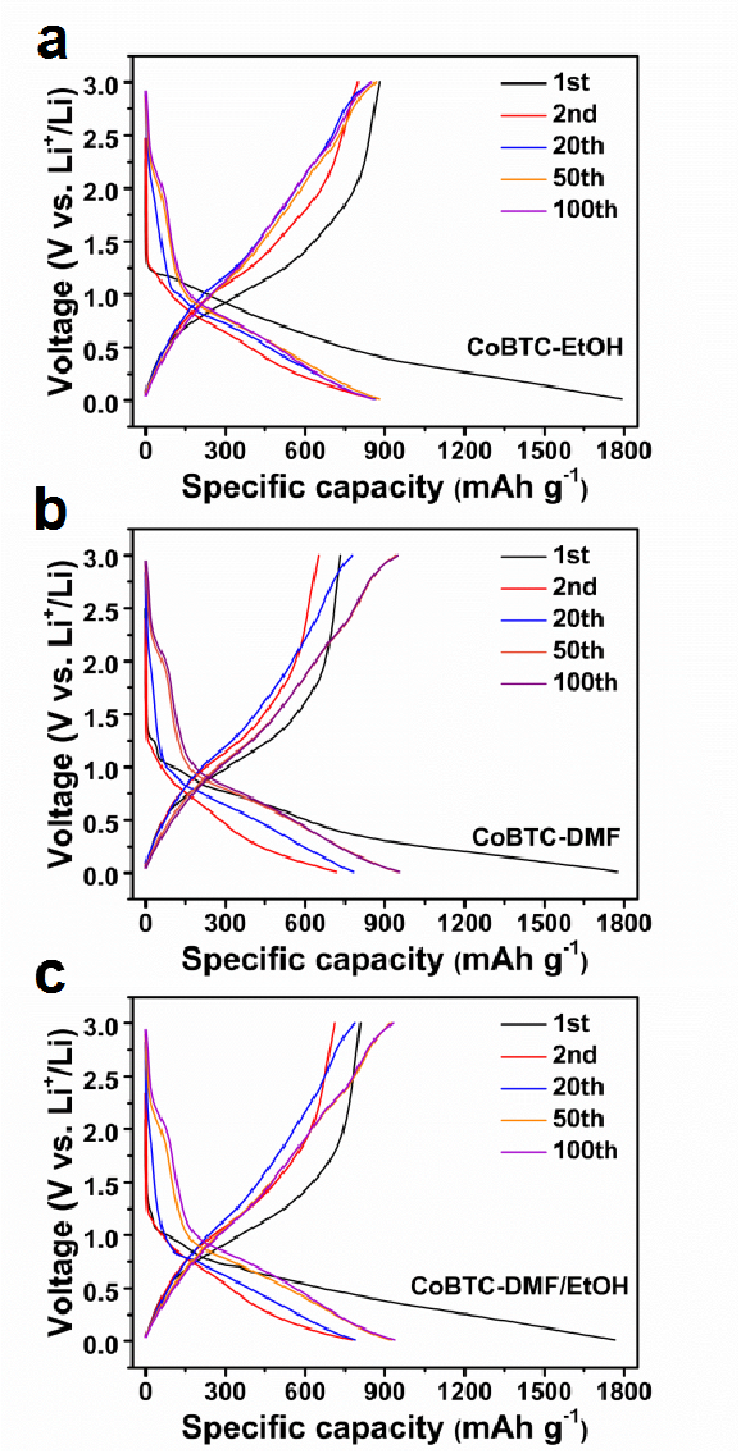

Figure S9. Galvanostatic charge-discharge profiles for CoBTC-EtOH (a), CoBTC-DMF (b), and CoBTC-DMF/EtOH (c) at a current density of 100 mA g^{-1}. From the 2nd to 50th cycle, the feature at ~2V *vs.* Li/Li^+ becomes more and more evident, and then become nearly unchanged after 50 cycles. Moreover, the discharge

and charge profiles for CoBTC-EtOH, CoBTC-DMF, and CoBTC-DMF/EtOH are similar after a significant number of cycles, indicating that similar redox reactions are occurring during the charging/discharging processes.

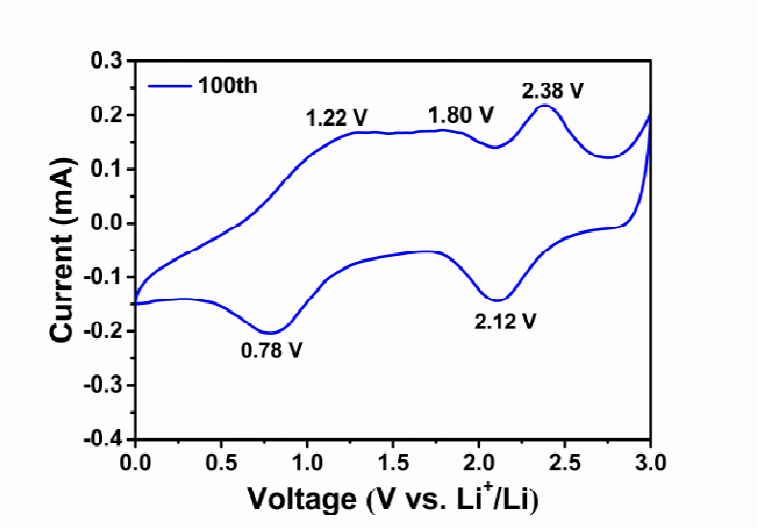

Figure S10. Cyclic voltammetry curve for CoBTC-EtOH after 100 cycles at a scan rate of 0.2 mV s^{-1} . Two broad cathodic peaks are observed at ~0.78 V and ~2.12 V, while three anodic peaks are observed at ~1.22 V, ~1.80 V, and ~2.38V. The broad nature of the redox peaks is probably indicative of gradual multi-step Li^+ insertion/deinsertion process. The cathodic peaks centered at 0.78 V and the anodic peaks at 1.22 V, and 1.80 V should be derived from the peaks at ~0.56 V, ~1.08V (cathodic peaks) and 1.77, 1.30 V (anodic peaks) from the 2nd CV cycle, and the positive shift of these redox peaks might be related to some activation processes for the Li-ion insertion. The new pair of peaks at ~2.12 V and ~2.38 V might be related with a new redox process after a significant number of charge-discharge cycles, which conincide well with the 100th galvanostatic charge-discharge profile in Figure S9a.

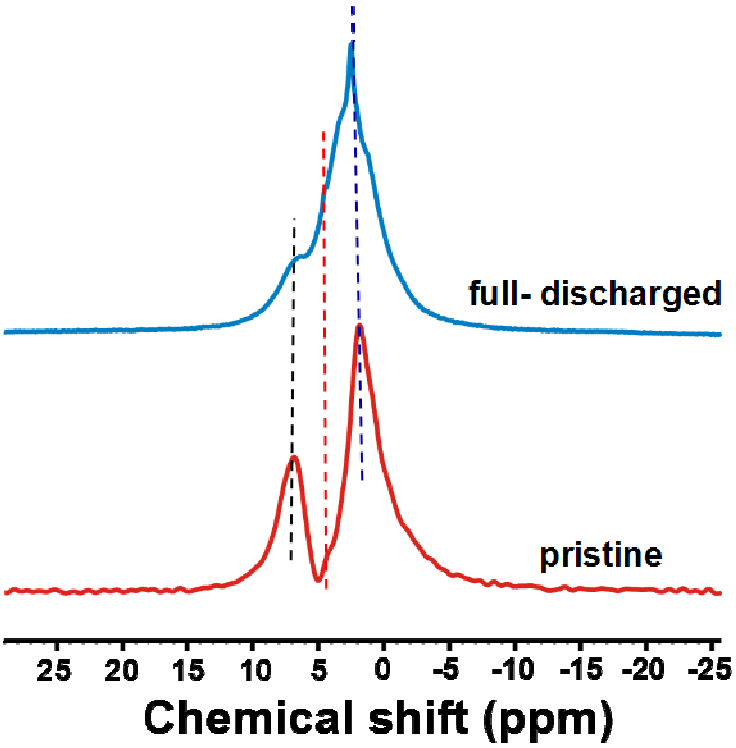

Figure S11. ^{1}H MAS NMR spectra of the pristine and fully-discharged CoBTC-EtOH electrodes. The ^{1}H signal from PVDF binder (2.7 ppm) is covered by the signal from CoBTC-EtOH, the ^{1}H signals located at 6.91, 4.29, and 1.91 ppm can be assigned to the three kinds of tertiary ^{1}H in the benzene rings of CoBTC-EtOH. It is clearly observed that after Li^{+} insertion to 0.01 V, the shape of the ^{1}H spectrum presents obvious variation, and the signal located at 1.91 ppm is shifted to 2.19 ppm, indicating that that Li-ions are incorporated with the benzene rings (H atoms are only exsited in the benzene rings).

Table S1. Metal organic frameworks or coordiantion polymers as anode materials in Li-ion battery

MOFs	Voltage window (V vs. Li/Li^+)	Rate (C or mA g^{-1})	Capacity retention (mAh g^{-1})	Cycle number	Refs.
Zn_4O(1,3,5-benzenetribenzoates)	0.05-1.6	50	105	50	[S1]
Li terephthalate	0.7-3.0	1C	234	50	[S2]
$Zn_3(HCOO)_6$	0.005-3.0	60	560	60	[S3]
Li/Ni-1,4,5,8-naphthalenetetracarboxylates	0.01-3.0	100	475	80	[S4]
Mn(tfbdc)(4,4'-bpy)$(H_2O)_2$)	0.01-2.5	50	390	50	[S5]
$Co_2(OH)_2$BDC	0.005-3.0	50	650	100	[S6]
$[Li_6(pda)_3]\cdot 2$EtOH	0.2-2.0	30	160	50	[S7]
$[Cu_2(C_8H_4O_4)_4]_n$	0.01-2.5	24	227	50	[S8]
2,6-Naph-$(COOLi)_2$	0.5-2.0	1C	ca. 210	10	[S9]
Ni-Me_4bpz	0.01-3.0	50	120	100	[S10]
$Zn(IM)_{1.5}(abIM)_{0.5}$	0.01-3.0	100, 400	190, ca. 75	200, 200	[S11]
Asp-Cu	0.01-3.0	50	233	100	[S12]
Mn-BTC	0.01-2.0	103, 1030	694, 400	100, 100	[S13]
Co 2,5-furandicarboxylate	0.01-3.0	100, 1250	549.8, 513.4	95, 499	[S14]
Mn 2,5-thiophenedicarboxylate	0.01-3.0	400	647.5	250	[S15]
Cu-BTC	0.05-3.0	96, 383	740, 474	50, 50	[S16]
This work	0.01-3.0	100, 2000	856, 473	100, 500	

Supplementary References

[S1] Li, X.; Cheng, F.; Zhang, S.; Chen, J. Shape-Controlled Synthesis and Lithium-Storage Study of Metal-Organic Frameworks Zn_4O(1,3,5-benzenetribenzoate)$_2$. *J. Power Sources* **2006**, *160*, 542-547.

[S2] Armand, M.; Grugeon, S.; Vezin, H.; Laruelle, S.; Ribière, P.; Poizot, P.; Tarascon, J. M. Conjugated Dicarboxylate Anodes for Li-Ion Batteries, *Nat. Mater.* **2009**, *8*, 120-125.

[S3] Saravanan, K.; Nagarathinam, M.; Balaya, P.; Vittal, J. J. Lithium Storage in a Metal Organic Framework with Diamondoid Topology-A Case Study on Metal Formates, *J. Mater. Chem.* **2010**, *20*, 8329-8335.

[S4] Han, X.; Yi, F.; Sun, T.; Sun, J. Synthesis and Electrochemical Performance of Li and Ni 1,4,5,8-Naphthalenetetracarboxylates as Anodes for Li-Ion Batteries, *Electrochem. Commun.* **2012**, *25*, 136-139.

[S5] Liu, Q.; Yu, L.; Wang, Y.; Ji, Y.; Horvat, J.; Cheng, M.; Jia, X.; Wang, G. Manganese-Based Layered Coordination Polymer: Synthesis, Structural Characterization, Magnetic Property, and Electrochemical Performance in Lithium-Ion Batteries. *Inorg. Chem.* **2013**, *52*, 2817-2822.

[S6] Gou, L.; Hao, L.; Shi, Y. X.; Ma, S.; Fan, X.; Xu, L.; Li, D.; Wang, K. One-Pot Synthesis of a Metal-Organic Framework as an Anode for Li-Ion Batteries with Improved Capacity and Cycling Stability. *J. Solid State Chem.* **2014**, *210*, 121-124.

[S7] Liu, Q.; Yu, L.; Wang, Y.; Ji, Y.; Horvat, J.; Cheng, M.; Jia, X.; Wang, G. Manganese-Based Layered Coordination Polymer: Synthesis, Structural Characterization, Magnetic Property, and Electrochemical Performance in Lithium-Ion Batteries. *Inorg. Chem.* **2013**, *52*, 2817-2822.

[S8] Kumar, R. S.; Nithya, C.; Gopukumar, S.; Anbu, M. Diamondoid-Structured Cu-Dicarboxylate-Based Metal-Organic Frameworks as High-Capacity Anodes for Lithium-Ion Storage, *Energy Technology* **2014**, *2*, 921-927.

[S9] Ogihara, N.; Yasuda, T.; Kishida, Y.; Ohsuna, T.; Miyamoto, K.; Ohba, N. Organic Dicarboxylate Negative Electrode Materials with Remarkably Small Strain for High-Voltage Bipolar Batteries. *Angew. Chem. Int. Ed.* **2014**, *53*, 11467-11472.

[S10] An, T.; Wang, Y.; Tang, J.; Wang, Y.; Zhang, L.; Zheng, G. A Flexible Ligand-Based Wavy Layered Metal-Organic Framework for Lithium-Ion Storage. *J. Colloid Interf. Sci.* **2015**, *445*, 320-325.

[S11] Lin, Y.; Zhang, Q.; Zhao, C.; Li, H.; Kong, C.; Shen, C.; Chen, L. An Exceptionally Stable Functionalized Metal-Organic Framework for Lithium Storage. *Chem. Commun.* **2015**, *51*, 697-699.

[S12] Zhao, C.; Shen, C.; Han, W. Metal-Organic Nanofibers as Anodes for Lithium-Ion Batteries, *RSC ADV.* **2015**, *5*, 20386-20389.

[S13] Maiti, S.; Pramanik, A.; Manju, U.; Mahanty, S. Reversible Lithium Storage in Manganese 1,3,5-Benzenetricarboxylate Metal-Organic Framework with High Capacity and Rate Performance. *ACS Appl. Mater. Interfaces* **2015**, *7*, 16357-16363.

[S14] Fei, H.; Liu, X.; Li, Z. Hollow Cobalt Coordination Polymer Microspheres: A Promising Anode Material for Lithium-Ion Batteries with High Performance. *Chem. Eng. J.* **2015**, *281*, 453-458.

[S15] Fei, H.; Liu, X.; Li, Z.; Feng, W. Synthesis of Manganese Coordination Polymer Microspheres for Lithium-Ion Batteries with Good Cycling Performance. *Electrochim. Acta* **2015**, *174*, 1088-1095.

[S16] Maiti, S.; Pramanik, A.; Manju, U.; Mahanty, S. Cu_3(1,3,5-benzenetricarboxylate)$_2$ Metal-Organic Framework: A Promising Anode Material for Lithium-Ion Battery. *Micropor. Mesopor. Mater.* **2016**, *226*, 353-359.